Current Problems in Surgery 82 (2026) 102132

Contents lists available at ScienceDirect

Current Problems in Surgery

journal homepage: www.elsevier.com/locate/cpsurg

ORIGINAL ARTICLE

Frozen–thawed allogeneic fibroblast cell sheets enhance anastomotic healing in a rat colonic anastomotic leakage model

Akihiro Fujita, MD[a,b], Koji Ueno, PhD[a,b,c,*], Yoshihiro Takemoto, MD, PhD[a], Hiroshi Kurazumi, MD, PhD[a], Yuya Tanaka, MD, PhD[a], Junichi Murakami, MD, PhD[a,c], Yutaka Aoki, MS[d], Atsunori Oga, MD, PhD[e], Taro Takami, MD, PhD[b,c,f], Kimikazu Hamano, MD, PhD[a,b,c]

Introduction

Anastomotic leakage remains a major postoperative complication in gastrointestinal surgery regardless of the continuous efforts to reduce its incidence. Colorectal anastomotic leakage, occurring in approximately 3% to 10% of patients,[1-3] is associated with severe clinical conditions, including peritonitis, sepsis, reoperation, prolonged hospitalization, increased healthcare costs, and reduced quality of life. Various perioperative strategies—such as intraoperative indocyanine green fluorescence imaging to assess blood flow,[4] mechanical and chemical bowel preparation,[5] transanal drain placement,[6] and diverting ileostomy[7]—have been used to reduce the risk of anastomotic leakage. However, these approaches mainly target perioperative risk reduction and cannot achieve complete prevention. Furthermore, no existing strategy has focused on actively enhancing anastomotic healing through active biological reinforcement at the anastomotic site.

Our research group has focused on fibroblast sheet technology, a regenerative approach that promotes wound healing. Using a proprietary method for fabricating multilayered fibroblast sheets,[8] we initially established therapeutic efficacy in refractory cutaneous ulcers using autologous cell sheets,[8-11] followed by the development of allogeneic cell sheets to overcome the

From the [a]Department of Surgery and Clinical Science, Yamaguchi University Graduate School of Medicine, Ube, Japan; [b]Department of Tissue Regenerative Medicine, Faculty of Medicine and Health Sciences, Yamaguchi University, Ube, Japan; [c]Division of Advanced Cell Therapy, Research Institute for Cell Design Medical Science, Yamaguchi University, Ube, Japan; [d]New-STEP Research Center, Central Glass Co., Ltd., Kawagoe, Japan; [e]Department of Molecular Pathology, Yamaguchi University Graduate School of Medicine, Ube, Japan; and [f]Department of Gastroenterology and Hepatology, Yamaguchi University Graduate School of Medicine, Ube, Japan

* Address reprint requests to Koji Ueno, PhD, Department of Surgery and Clinical Science, Yamaguchi University Graduate School of Medicine, Minami-kogushi 1-1-1, Ube, Yamaguchi 755-8505, Japan.

E-mail address: kjueno@yamaguchi-u.ac.jp (K. Ueno).

https://doi.org/10.1016/j.cpsurg.2026.102132

limitations in obtaining high-quality autologous cells. Furthermore, allogeneic fibroblast sheets have exhibited wound-healing effects comparable to those of autologous fibroblast sheets in a murine cutaneous defect model,[12] and the therapeutic benefits of fibroblast sheets have been reported in models of esophageal reconstruction,[13] pancreatic fistula,[14] and bronchial leakage.[15] Moreover, to reduce the cost of cell sheet transplantation, the preservation of allogeneic fibroblast sheets is desirable. To address this, we developed a cryopreservation method using a three-dimensional (3D) freezer (KOGASUN Co., Ltd., Yamaguchi, Japan).[16] Conventionally, cell sheets are manufactured and transplanted to target sites using specialized devices. Therefore, we developed CY-1 (Central Glass Co., Ltd., Tokyo, Japan), a substrate that enables the fabrication and transplantation of cell sheets. By combining CY-1 with the 3D cryopreservation method, we revealed that cryopreserved fibroblast sheets can be readily transplanted after thawing,[17] and confirmed their efficacy in murine skin defects and rat esophageal reconstruction models.[17,18] Herein, we investigated the early-phase biological processes underlying anastomotic healing. The colon served as a representative gastrointestinal organ with a well-defined multilayered structure involving the mucosa, submucosa, muscularis propria, subserosa, and serosa, reflecting the typical architecture of reconstructive gastrointestinal tissues. We evaluated fibroblast sheet transplantation in a colonic anastomosis model with preserved multilayered gastrointestinal architecture and investigated its therapeutic effects on anastomotic leakage. Along with assessing functional outcomes such as anastomotic leakage and bursting pressure, we analyzed histological and molecular changes associated with early tissue repair. Specifically, collagen deposition across different tissue layers and its relationship with mechanical strength was investigated, providing insight into which anatomical layer contributes to anastomotic integrity. We also explored potential cellular responses, including vimentin expression and TGF-β1/pSMAD2 signaling as possible contributors to early healing processes. Through this integrative approach, this study aimed to clarify the mechanisms underlying anastomotic healing enhancement by fibroblast sheet transplantation and to provide a basis for its potential clinical application.

Materials and methods

Animals

Male Wistar/ST, Sprague–Dawley (SD), and SD-Tg rats—aged 8 to 12 weeks—were procured from Japan SLC Inc. (Shizuoka, Japan). The animals were maintained under controlled environmental conditions (temperature 22 °C ± 2 °C, humidity 70% ± 20%, and 12-hour light/dark cycle) with ad libitum access to food and water. All experimental procedures were conducted in accordance with institutional guidelines and approved by the Institutional Animal Care and Use Committee of Yamaguchi University (approval no. 31-007). All procedures, including analgesia, euthanasia, and donor tissue harvesting, conformed to the institutional and national guidelines and were approved by the Institutional Animal Care and Use Committee. Efforts to minimize animal use and refine experimental procedures were taken in accordance with the principles of the 3Rs. Although animals were allocated to experimental groups without formal randomization (Supplementary Fig. 1), all were maintained under identical environmental and experimental conditions, with procedures performed according to a strictly standardized protocol to minimize variability. Group assignments were not concealed from the surgeon during allocation. However, outcomes were assessed in a blinded manner to minimize potential bias. Given the nature of the intervention, the surgeon could not be blinded.

Preparation of cryopreserved multilayered fibroblast sheets

Cryopreserved multilayered fibroblast cell sheets were prepared as previously described.[18] Oral mucosal tissues were harvested from 8 to 12-week-old SD and SD-Tg rats under anesthesia

with 5% isoflurane for induction and 2% for maintenance (MSD Animal Health, Tokyo, Japan). Tissues were minced and incubated in Dulbecco's Modified Eagle's Medium (Thermo Fisher Scientific, Waltham, MA, USA) supplemented with 10% fetal bovine serum (FBS), 5% collagenase (FUJIFILM Wako Pure Chemical Corp., Osaka, Japan), and 1% penicillin–streptomycin at 37 °C in 5% CO_2. Following overnight incubation, the medium was centrifuged, supernatant was removed, and residual tissue fragments were cultured for an additional 3 days. Cells were subsequently collected using 0.05% trypsin–EDTA and passed through a 40-μm cell strainer to remove remaining tissue fragments. After centrifugation, the isolated cells were cultured for 4 days. Fibroblast identity was confirmed according to characteristic spindle-shaped morphology and positive vimentin immunostaining. A sterilized CY-1 thermoplastic culture substrate (Central Glass Co., Ltd., Tokyo, Japan) was affixed to the bottom of a 48-well plate. CY-1 is a hydrophilic-treated thermoplastic resin film designed to support multilayered sheet formation. Fibroblasts (2.5×10^5 cells/well) were seeded onto the CY-1 surface. After 24 hours, the medium was replaced with CTS AIM-V SFM (Thermo Fisher Scientific, Waltham, MA, USA) supplemented with HFDM-1 (+) medium (Cell Science & Technology Institute, Miyagi, Japan) containing 5% FBS. On the following day, after removing the medium, 150 μL/well of the cryopreservation solution Bambanker hRM (GC Lymphotec Inc., Tokyo, Japan) was added. Plates were frozen at −35 °C for 30 minutes using a 3D freezer and then transferred to a −80 °C freezer for storage until further use.

Colonic anastomosis model

A colonic anastomotic leakage model was established according to previously reported methods.[19,20] Male Wistar/ST rats (8-12 weeks old) were anesthetized with isoflurane (5% for induction, 2% for maintenance). Following abdominal shaving, a 4-cm midline laparotomy was performed. The small intestine and cecum were exteriorized to the right side and then covered with a saline-moistened gauze. The distal colon, located 5 to 10 mm distal to the left renal artery and serving as an anatomical landmark, was transected. No bowel preparation or dietary restriction was introduced. If present, fecal material at the intended transection site was gently milked distally using nontoothed forceps. The marginal vessels and vasa recta were not ligated to preserve intestinal blood flow. A four-interrupted-suture anastomosis was constructed using 6-0 polypropylene sutures (Medtronic, Minneapolis, MN, USA), which were placed at standardized positions (antimesenteric side, mesenteric side, and the anterior and posterior wall midpoints) at equal intervals. The small intestine and cecum were then returned to their original positions, followed by abdominal wall closure. No fasting period was applied; thus, animals were allowed free access to food and water throughout the perioperative period. All procedures were performed by the same surgeon (A.F.) to ensure consistency. Exclusion criteria included intraoperative death and unintended transection or injury to the intestinal vessels, including the marginal vessels and vasa recta. No animals met these criteria; hence, none were excluded.

Transplantation of frozen–thawed sheets

Two multilayered fibroblast sheets were thawed on the CY-1 substrate at room temperature for 30 minutes. The sheets were then circumferentially applied to the anastomotic site, covering the ventral and dorsal surfaces. Before sheet application, excess moisture on the serosal surface was carefully removed using gauze to facilitate adhesion to this surface. Next, by gently pressing the CY-1 substrate against the tissue and maintaining contact for approximately 30 seconds, adhesion was achieved. In this transplantation method, fibroblasts cultured on the CY-1 substrate adhered directly to the target site, after which the CY-1 substrate was removed, leaving only the cell sheet on the tissue.[17,18] No sutures or adhesives were used for fixation. Characteristic whitish appearance of the serosal surface after sheet application macroscopically confirmed circumferential coverage.

Perioperative analgesia, monitoring, and humane endpoints

Analgesia was induced preoperatively using buprenorphine (0.1 mg/kg, subcutaneously). Postoperative analgesia was provided as needed according to daily clinical assessment, in accordance with institutional guidelines.

Animals' general condition, including activity level, posture, grooming behavior, food and water intake, and signs of pain or distress (eg, piloerection, decreased mobility, or abdominal guarding), were monitored at least once daily.

Humane endpoints were predefined as follows: severe lethargy or inability to ambulate, persistent anorexia or dehydration, signs of severe infection or peritonitis, or any condition indicating no possibility to recover. Animals meeting these criteria were humanely euthanized.

Within the study period, no animals met these endpoint criteria.

Assessment of anastomotic leakage, bursting pressure, and histology

The primary outcome was anastomotic leakage rate, defined as an Anastomotic Complication Score (ACS) of $\geq$3 points. ACS, bursting pressure, and histological assessments constituted the secondary outcomes.

Rats were euthanized on postoperative day (POD) 3. Anastomotic healing was evaluated using the ACS,[21] a macroscopic scoring system ranging from 0 to 6, with a score of $\geq$3 indicating leakage, defined as follows:

Score 0: No adhesions or abnormalities.
Score 1: Adhesions to the fat pad with a clean anastomosis underneath.
Score 2: Adhesions to an intestinal loop, abdominal wall, or another organ.
Score 3: Anastomotic defect identified beneath the adhesion, without other abnormalities.
Score 4: Evidence of possible contamination, such as small abscesses.
Score 5: Clear anastomotic complications, including pus dissemination, obstruction at the anastomosis, or signs of peritonitis.
Score 6: Fecal peritonitis or death resulting from peritonitis.

Bursting pressure was measured according to previously described methods.[13] A colonic segment involving the anastomosis was isolated, with 1 cm on both the oral and anal sides. Both ends were ligated at 2 mm from the cut edges using 4-0 nylon sutures (Nicho Co., Tokyo, Japan). The resected colon was then submerged in water and connected to a nonmercury sphygmomanometer (HT-1500; Nippon Seimitsu Sokki Co., Gunma, Japan) via a 24G catheter. Air was insufflated manually at a rate as slow and constant as possible, and the first pressure peak associated with leakage was recorded as the bursting pressure. The manometer was checked to ensure a zero reading under atmospheric pressure before each measurement, and the same device was used for all measurements. The rupture site was also visually confirmed during measurement, located at the anastomosis in all cases.

Leakage incidence and bursting pressure were evaluated in 30 rats (15 per group). Of these rats, the last 5 animals in each group were utilized for histological analysis. Furthermore, tissue sections underwent Azan staining to evaluate collagen deposition at the anastomotic site. For layer-specific analysis, the intestinal wall was divided into mucosal, submucosal, and subserosal regions. We defined the submucosal region as the area between the muscularis mucosae and the muscularis propria, and the subserosal region as the area between the outer border of the muscularis propria and the serosal surface. The area extending 500 μm orally and anally from the center of the anastomosis defined the region of interest (ROI). For the quantitative analysis of collagen deposition, the Azan-positive area within each predefined region was measured using the ImageJ software (NIH, Bethesda, MD, USA). Color thresholding was applied with the following parameters: hue, 140 to 200; saturation, 40 to 255; and brightness, 0 to 255. Binarized images were used for area measurement, with the same threshold settings applied to ensure consistency across samples.

Tissues were fixed in 10% neutral buffered formalin (FUJIFILM Wako Pure Chemical Corp., Osaka, Japan), embedded in paraffin, and then sectioned for hematoxylin–eosin (H&E) and Azan staining.

In accordance with the institutional guidelines, euthanasia was performed by inhalation of isoflurane overdose.

Investigators who were blinded to group allocation performed the outcome assessments, including ACS and bursting pressure measurements.

Histological analysis

Rats were euthanized at 15 min and on POD 1, 5, and 9, and the colonic anastomotic site was harvested. All histological evaluations were performed exclusively on grossly intact, nonleakage anastomotic sites. Tissues were fixed in 10% neutral buffered formalin (FUJIFILM Wako Pure Chemical Corp., Osaka, Japan), embedded in paraffin, and sectioned for H&E staining, Azan staining, and immunofluorescence (IF) analysis. IF staining was performed on specimens collected at POD 5. The following primary antibodies were used: anti-GFP polyclonal antibody (598; MBL Co., Ltd., Aichi, Japan), anti-TGF-β1 antibody (ab215715; Abcam, Cambridge, UK), antiphospho-Smad2 (Thr220) antibody (Abcam, Cambridge, UK), antivimentin antibody (ab8069, 1:500; Abcam, Cambridge, UK), and anti-C-ERC/mesothelin antibody (306; #28001; Immuno-Biological Laboratories, Gunma, Japan). Secondary antibody was DyLight® 550–conjugated goat antirabbit immunoglobulin G (ab96884; Abcam, Cambridge, UK). Nuclei were counterstained with DAPI (Bio-Rad Laboratories, Hercules, CA, USA). Images were captured using a BZ-X710 microscope (Keyence Corp., Osaka, Japan) and analyzed using BZ-X Analyzer software (Keyence Corp.). For immunofluorescence analyses, ROIs were defined at the anastomotic site. Two microscopic fields per section (oral and anal sides relative to the anastomotic center) were evaluated for TGF-β1/pSmad2 coexpression analysis, and 3 microscopic fields within the subserosal region for vimentin analysis. One section per animal was used for all analyses. Individual animal served as the unit of analysis. Measurements obtained from multiple fields were averaged to generate a single representative value per animal, preventing pseudoreplication. Positive cells were defined using fixed fluorescence intensity thresholds, with 38 for TGF-β1/pSmad2 and 50 for vimentin, and DAPI was used for nuclear identification. Identical imaging settings, including exposure times (17, 20, 14, and 1/3 seconds for TGF-β1, pSmad2, vimentin, and DAPI), were applied across all samples. A pathologist (A.O.) blinded to group allocation and treatment conditions conducted the histological and immunofluorescence analyses.

A total of 25 rats were used. One rat was euthanized at 15 minutes, and 24 rats were allocated to either the control or cell sheet groups, with 4 rats per group at each time point (POD 1, 5, and 9). All animals were euthanized by inhalation of isoflurane overdose, in accordance with institutional guidelines.

Measurement of the muscularis gap at the colonic anastomotic site

The muscularis gap at the anastomotic site was quantified by identifying the edges of the muscularis propria and drawing perpendicular reference lines at these boundaries. The shortest distance between the 2 lines was measured using ImageJ software (National Institutes of Health, Bethesda, MD, USA).

Statistical analysis

The primary outcome of this study was anastomotic leakage, defined as an ACS of $\geq$3. Secondary outcomes included the ACS as an ordinal variable, bursting pressure, histological assessments, and muscularis gap measurements.

Statistical analyses were conducted using JMP Pro version 18 (SAS Institute Inc., Cary, NC, USA) and GraphPad Prism 10 software (GraphPad Software, Boston, MA, USA). Continuous variables were expressed as mean ± standard deviation for normally distributed data and as median with interquartile range for non-normally distributed data. Given the ordinal nature of ACS, group differences were evaluated using an ordinal logistic regression analysis (proportional odds model). For completeness, nonparametric comparisons using the Mann–Whitney U test were performed as well. Leakage incidence was compared using Fisher's exact test. Absolute risk differences and corresponding 95% confidence intervals were calculated using the normal approximation (Wald method), in addition to *P*-values. Differences between groups for continuous variables were assessed using Student's *t*-test or the Mann–Whitney U test, as appropriate. Longitudinal changes in muscularis gap measurements (POD 1, 5, and 9) were analyzed using two-way analysis of variance (ANOVA). For immunofluorescence analyses, statistical comparisons were performed using binomial logistic regression based on per-animal aggregated values. A *P*-value of <0.05 was considered statistically significant. As no formal *a priori* power calculation was performed, this study should be considered exploratory in nature.

No data were missing in this study. If missing data had arisen, complete-case analysis would be conducted.

Results

Histological analysis and persistence of frozen–thawed GFP-expressing multilayered fibroblast sheets after transplantation

Fig. 1A-D illustrates the histological appearance of frozen–thawed GFP-expressing multilayered fibroblast sheets transplanted onto the rat colonic anastomosis. H&E and Azan staining of specimens harvested 15 minutes after implantation revealed that the thawed sheets retained their multilayered structure, measuring approximately 30 μm in thickness and comprising 3 to 4 fibroblast layers.

Histopathological images from H&E and Azan staining were obtained at POD 0, 1, 5, and 9 (Fig. 1E, F). IF analysis of frozen–thawed GFP-expressing multilayered fibroblast sheets after transplantation over time (POD 0–POD 9) is illustrated in Fig. 1G. GFP-expressing sheet structures were clearly observed on POD 0 and POD 1. By POD 5, GFP-expressing cells were still detectable at very low levels, although the sheet structure was no longer maintained. No GFP-expressing cells were observed on POD 9. Quantitative analysis of GFP-positive area showed a marked decrease over time (POD 0: 66,522 μm²; POD 1: 2,665 μm²; POD 5: 1,931 μm²; POD 9: 595 μm²). These results indicate that frozen–thawed multilayered fibroblast sheets gradually degrade and disappear following transplantation.

Evaluation of the anastomotic site following frozen–thawed multilayered fibroblast sheet transplantation

After euthanasia on POD 3, the anastomotic site was evaluated. The rate of anastomotic leakage (defined as ACS $\geq$ 3)—the primary outcome—was significantly reduced in the fibroblast sheet group compared with that in the control group (26.7% vs 73.3%, $P = 0.027$), corresponding to an absolute risk difference of −46.7% (95% CI, −78.3% to −15.0%) (Table 1). Additionally, ACS distribution was significantly lower in the fibroblast sheet group (median: 2.0 [IQR 1.0–3.0] vs 4.0 [IQR 2.5-4.0]; median difference: −2.0, 95% CI: −3.0 to 0.0; $P = 0.01$) (Fig. 2A). Representative intraoperative images corresponding to ACS evaluations are shown in Fig. 2B. Furthermore, ordinal logistic regression analysis demonstrated that the fibroblast sheet group was significantly associated with lower ACS (odds ratio, 0.15: $P = 0.014$). Bursting pressure values were more consistent and tended to be higher in the fibroblast sheet group than

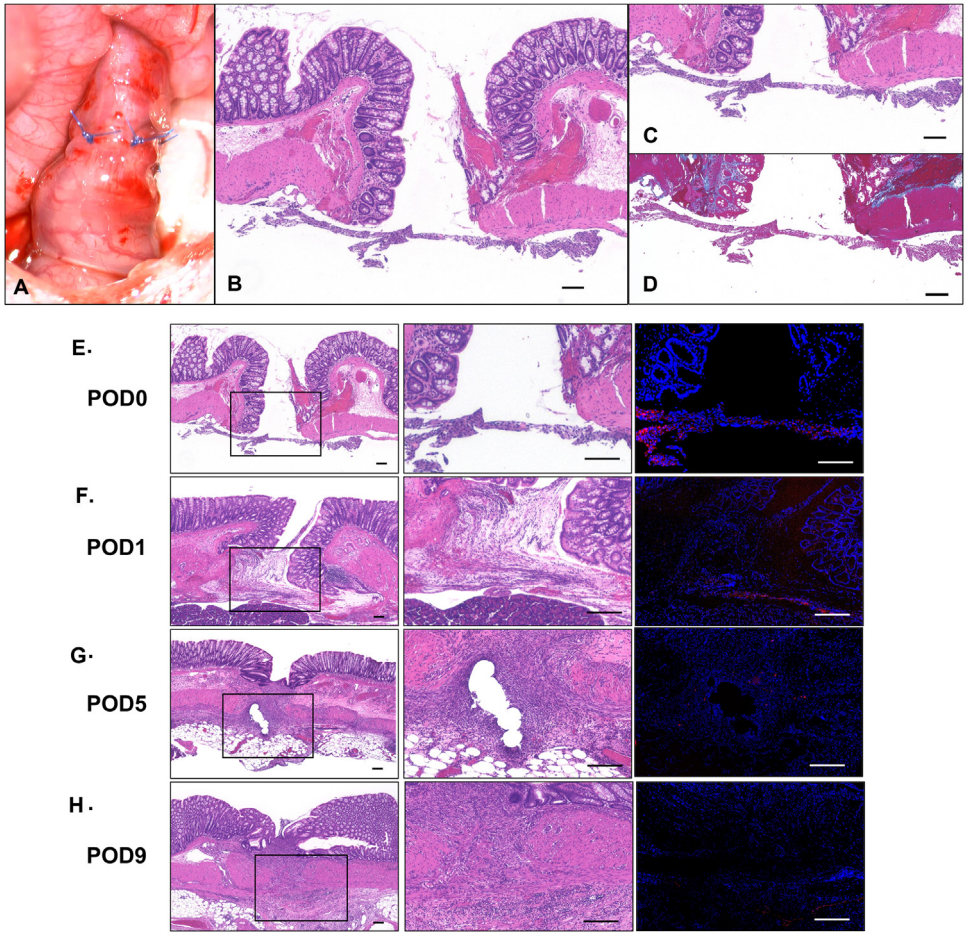

Fig. 1. Histological characteristics, persistence, and application of frozen–thawed GFP-expressing multilayered fibroblast sheets at the colonic anastomosis. (A) Intraoperative view showing a colonic anastomosis constructed with four interrupted sutures and circumferentially covered with a multilayered fibroblast cell sheet. (B) H&E staining of the anastomotic site 15 min after cell sheet transplantation. (C) High-magnification H&E image of the frozen–thawed multilayered fibroblast sheet in (B). (D) High-magnification Azan-stained image of the frozen–thawed multilayered fibroblast sheet in (B). (E-H) Time-course histological and immunofluorescence analyses of the anastomotic site. For each time point, low-magnification H&E (left), high-magnification H&E (middle), and immunofluorescence images showing GFP-expressing cells (right) are presented. (E) postoperative day (POD) 0; (F) POD 1; (G) POD 5; (H) POD 9. GFP-positive area decreased over time (POD 0: 66,522 μm²; POD 1: 2,665 μm²; POD 5: 1,931 μm²; POD 9: 595 μm²). Scale bars: 100 μm (B, E-H: left panels); 50 μm (C, D, E-H: middle and right panels).

Table 1
Incidence of anastomotic leakage and rat mortality rates.

	Control (n = 15)	Cell sheet (n = 15)	P-value
Anastomotic leakage	11/15 (73%)	4/15 (26%)	0.02
Mortality rate	0/15	0/15	–

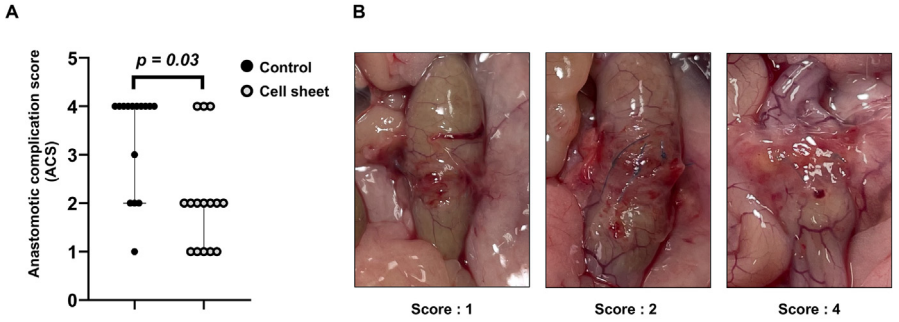

Table 1

	Control (n=15)	Cell sheet (n=15)	P-value
Anastomotic leakage	11/15 (73%)	4/15 (26%)	*0.02*
mortality rate	0/15	0/15	—

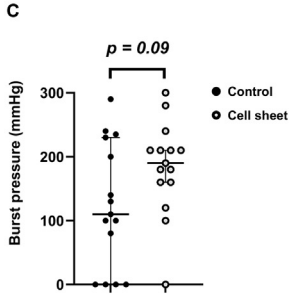

Fig. 2. Anastomotic complication score and bursting pressure on POD 3. (A) ACS. Each experimental group consisted of 15 animals evaluated on POD 3. (B) Representative intraoperative images illustrating ACS scores of 1, 2, and 4. (C) Bursting pressure resistance evaluation as a measure of anastomotic pressure resistance. Each experimental group consisted of 15 animals evaluated on POD 3.

in the control group (median: 190 mmHg [IQR 160-210] vs 110 mmHg [IQR 40-215]; median difference: 80 mmHg, 95% CI: −20 to 160 mmHg), although the difference did not reach statistical significance ($P = 0.09$) (Fig. 2C). Notably, several animals in the control group also exhibited relatively high bursting pressure values, resulting in increased variability within the group.

Histological evaluation of the colonic anastomotic site

Representative histological findings of the anastomotic site were assessed on PODs 1, 5, and 9 in both groups (Fig. 3A). Submucosal edema gradually decreased over time, whereas subserosal tissue thickening became increasingly apparent. Fig. 3B illustrates the representative measurement of the muscularis gap, which is quantified in Fig. 3C. Postoperative muscularis gap changes were analyzed using a two-way ANOVA (Fig. 3C). At all evaluated time points, the muscularis gap was significantly smaller in the fibroblast sheet group than in the control group ($P = 0.01$) (Fig. 3C). At each time point, the fibroblast sheet group consistently showed smaller values than the control group. The median differences (fibroblast sheet vs control) were 373, 614, and 571 μm (95% CI: 830 to 0, 1500 to 100, and 900 to 200 μm) at PODs 1, 5, and 9, respectively. Although the muscularis gap remained consistently smaller in the fibroblast sheet group on PODs 5 and 9, the rate of change in these time points did not differ significantly between the 2 groups. Therefore, fibroblast sheet transplantation may accelerate the approximation of the muscularis layers during the early postoperative period and maintain improved tissue integrity throughout the observation period.

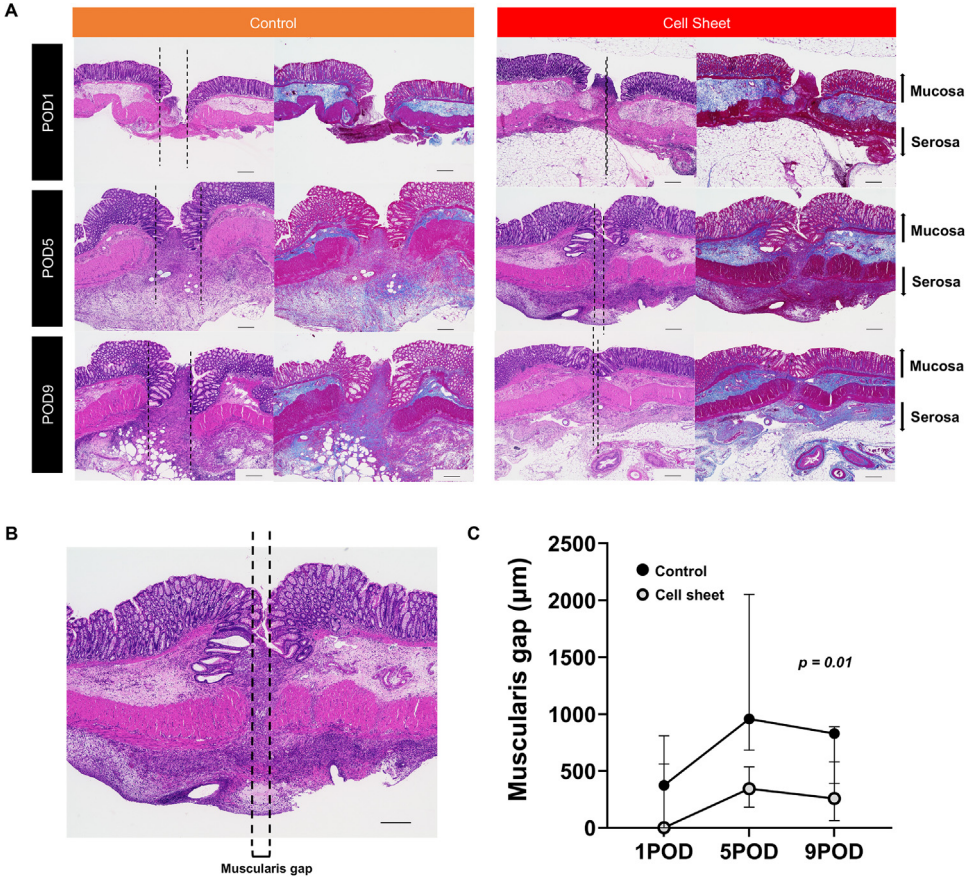

Fig. 3. Histological evaluation of the anastomotic site. (A) Representative histological images of the anastomotic site on POD 1, 5, and 9 in the control and fibroblast sheet groups. For each time point, the H&E-stained sections (left panels) and Azan-stained sections (right panels) are shown. Dashed lines indicate perpendicular reference lines drawn from the edges of the muscularis propria to visualize the muscularis gap. Scale bar: 100 μm. (B) Representative pathological histopathological images showing measurements of the muscularis gap, with dashed lines indicating the reference points used for quantification. Scale bar: 100 μm. (C) Quantitative evaluation of the muscularis gap on POD 1, 5, and 9. Data were analyzed using two-way ANOVA ($n = 4$ per group).

Collagen deposition at the anastomotic site evaluated by Azan staining

Collagen deposition at the anastomotic site on POD 3 was evaluated through Azan staining (Fig. 4A). Representative images show collagen accumulation in both groups, particularly within the submucosal and subserosal layers. Quantitative analysis revealed that the Azan-positive area in the mucosa or submucosa did not significantly differ between the 2 groups. Conversely, collagen deposition in the subserosal layer tended to be greater in the fibroblast sheet group than in the control group ($P = 0.09$) (Fig. 4B). Correlation analysis between Azan-positive area and bursting pressure demonstrated no significant association in the mucosal ($\rho = -0.08$, $P = 0.83$) and submucosal layers ($\rho = 0.06$, $P = 0.88$). However, we observed a significant positive correlation in the subserosal layer ($\rho = 0.64$, $P = 0.04$) (Fig. 4C).

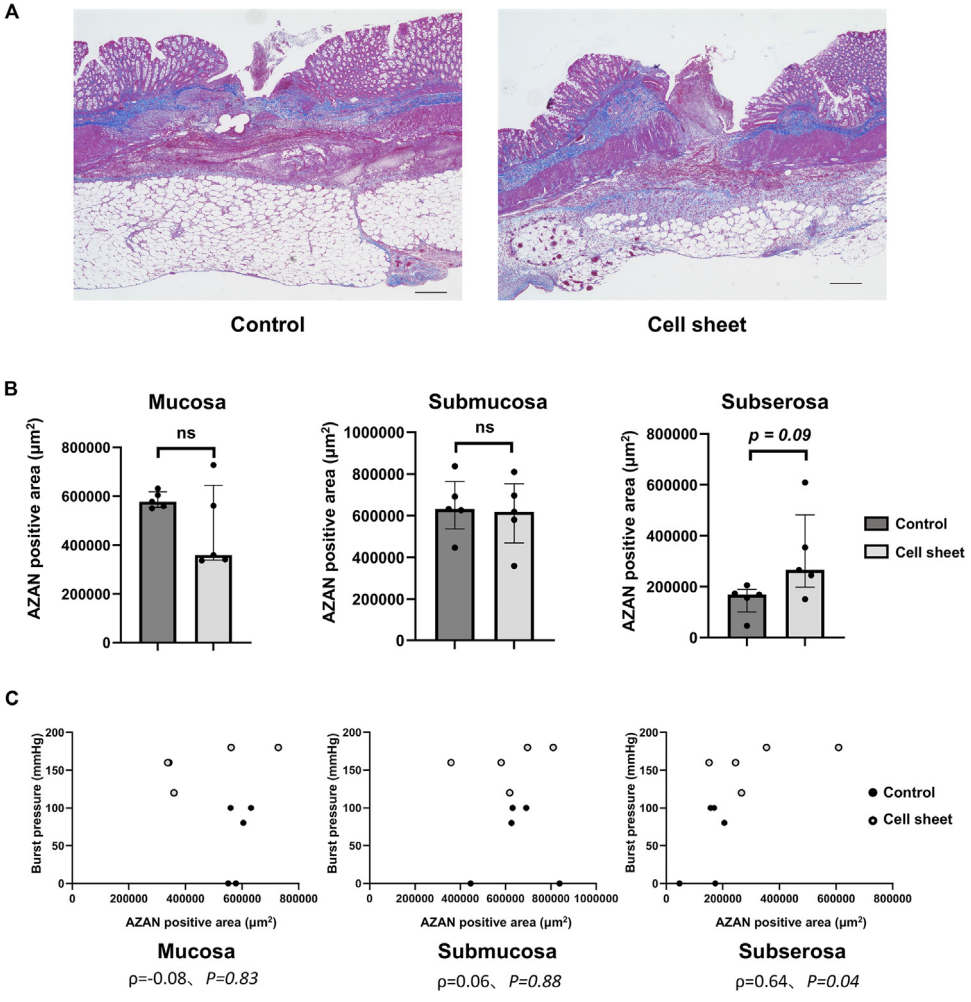

Fig. 4. Collagen deposition at the anastomotic site evaluated by Azan staining. (A) Representative Azan-stained images of the anastomotic site on POD 3 in the control and fibroblast sheet groups. Collagen fibers are stained blue, indicating that the collagen accumulated mostly in the submucosal and subserosal layers. Scale bar: 300 μm. (B) Quantitative analysis of Azan-positive areas in the mucosa, submucosa, and subserosa. For layer-specific analysis, the intestinal wall was divided into mucosal, submucosal, and subserosal regions. The submucosal region was the area between the muscularis mucosae and the muscularis propria, whereas the subserosal region was the area between the outer border of the muscularis propria and the serosal surface. Regions of interest were the areas extending 500 μm orally and anally from the center of the anastomosis. The Azan-positive areas were quantified using the ImageJ software. (C) Correlation between the bursting pressure and AZAN-positive areas in the mucosa, submucosa, and subserosa on POD 3 in the control and fibroblast sheet groups.

Comparison of vimentin-positive cells at the anastomotic site

Vimentin-positive cells in the subserosal region were analyzed on POD 5 (Fig. 4A, B). Logistic regression analysis revealed that the density of vimentin-positive cells was significantly higher in the fibroblast sheet group compared with the control group (odds ratio [OR] = 1.68; 95% confidence interval [CI] 1.50-1.88; $P < 0.01$) (Fig. 4B). These findings indicate the enhanced presence of mesenchymal cells at the anastomotic site following fibroblast sheet transplantation.

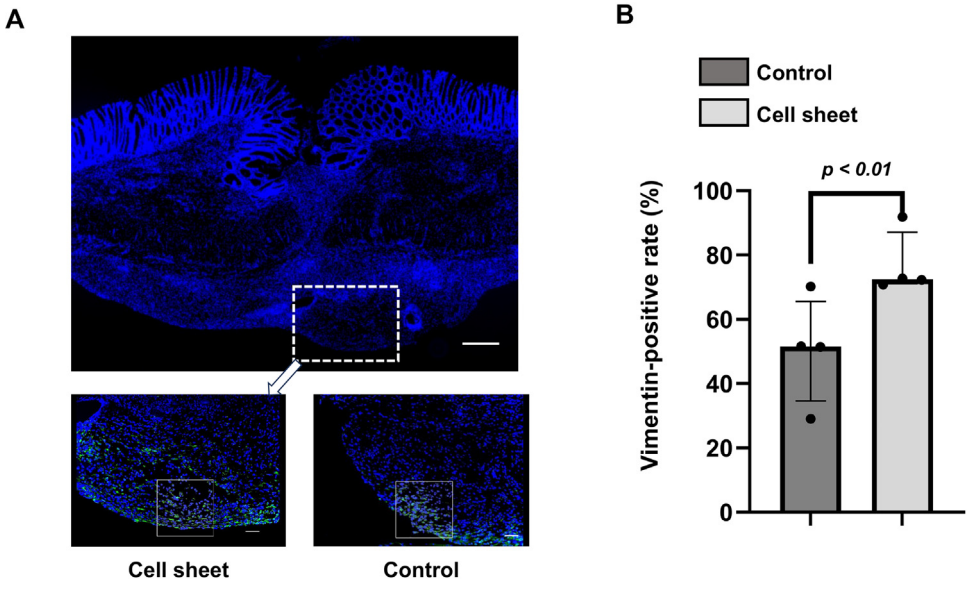

Fig. 5. Comparison of Vimentin-positive cells in the subserosal layer. (A) Vimentin-positive cells (green) and DAPI-stained nuclei (blue) were automatically quantified in 3 randomly selected subserosal regions (200 μm × 200 μm) per specimen using BZ-X Analyzer software. The upper figure panel shows typical immunofluorescence staining in the cell sheet on POD 5. The lower-left figure panel shows an enlarged view of the area within the white dotted line located in the subserosal layer of the upper figure. The lower-right figure panel depicts the same magnification as the one on the lower left and shows the area within the subserosal layer of the control. (B) The vimentin-positive cell ratio was calculated as the number of vimentin-positive cells divided by the total number of DAPI-positive nuclei. Group differences were analyzed using binomial logistic regression. Three randomly selected fields per specimen were analyzed ($n = 4$ per group). Scale bars: 50 μm.

Fluorescent immunostaining analysis of TGF-β1 and phosphorylated SMAD2 at the anastomotic site following cell sheet transplantation

Representative IF staining using anti-TGF-β1 and antiphospho-SMAD2 antibodies is shown in Fig. 5A for POD 5. Colocalized expression of TGF-β1 and phosphorylated SMAD2 was predominantly observed in the subserosal region of the anastomotic site and was rare in other regions. Therefore, colocalization was specifically quantified in the subserosal region (Fig. 5B). Logistic regression analysis revealed that the fibroblast sheet group exhibited significantly higher coexpression of TGF-β1 and phosphorylated SMAD2 compared with the control group (OR = 5.41; 95% CI: 3.42-8.54; $P < 0.01$). These findings indicate a statistically significant increase in TGF-β1/pSMAD2 coexpression at the subserosal region following fibroblast sheet transplantation.

Discussion

In this study, we evaluated the preventive effects and potential mechanisms of frozen–thawed allogeneic multilayered fibroblast cell sheet transplantation using a rat model of colonic anastomotic leakage. Compared with the control group, the fibroblast sheet group exhibited a significantly lower ACS (median: 4.0 [IQR 2.5-4.0] vs 2.0 [IQR 1.0–3.0]; $P = 0.01$) (Fig. 2A) as well as a lower incidence of anastomotic leakage (73% vs 26%; $P = 0.02$) (Table 1). Although fibroblast sheet transplantation exhibited a trend toward higher bursting pressure compared with the controls (Fig. 2C), this difference was not significant. This outcome may be attributable to the limited sample size, which was constrained by animal welfare considerations. Increasing the sam-

ple size could potentially reveal statistically significant differences in this outcome. These findings suggest that fibroblast sheet transplantation can reduce anastomotic leakage, potentially improving the bursting pressure. However, this finding should be interpreted as a preliminary positive signal that requires further validation. Histological analysis revealed that the muscularis gap at the anastomotic site was substantially smaller in the fibroblast sheet group on POD 5, and its widening remained suppressed on POD 9 (Fig. 3). Healing of colonic anastomoses is reported to follow processes similar to cutaneous wound healing, including inflammatory, proliferative, and remodeling phases, with temporal changes in tissue responses documented in rat models.[20] Vimentin serves as a marker for the activation and recruitment of fibroblasts, other mesenchymal cells, and epithelial–mesenchymal transition (EMT).[22,23] In this study, the proportion of vimentin-positive cells in the subserosal layer was higher in the fibroblast sheet group than in the control group (Fig. 4), suggesting that EMT-like changes may be present in the subserosal layer following fibroblast sheet transplantation. Vimentin has been reported to play an important role in wound healing, and its expression can be induced by TGF-β1 in fibroblasts.[24] Additionally, TGF-β1 has been shown to induce EMT through SMAD2 activation in epithelial cells,[25,26] and the TGF-β/Smad2 signaling pathway mediates EMT in mouse models.[27] Consistent with these findings, coexpression of TGF-β1 and phosphorylated SMAD2 in the anastomotic subserosa was increased in the fibroblast sheet group on POD 5 (Figs. 5 and 6), supporting the possibility of EMT-like changes in the subserosal layer. Gastrointestinal anastomoses commonly involve organs such as the stomach, small intestine, and colon, all of which possess a serosal layer composed of mesothelial cells. Mesothelial cells have been reported to contribute to tissue repair and may undergo phenotypic changes consistent with EMT,[28] and serosal cells have been reported to participate in anastomotic healing at gastrointestinal anastomotic sites.[29] Collectively, these data suggest possible phenotypic changes in epithelial or mesothelial cells in the subserosa; however, any involvement of EMT remains speculative.

Although this study did not directly evaluate growth factor secretion or extracellular matrix remodeling, previous studies have shown that rat multilayered fibroblast sheets secrete angiogenic factors such as hepatocyte growth factor and vascular endothelial growth factor, cytokines including TGF-β1, chemokines such as MCP-1, and matrix-remodeling molecules including matrix metalloproteinases and tissue inhibitors of metalloproteinases.[13,15] These sheets have also been shown to promote early collagen I deposition.[18] MCP-1 has been reported to induce M2 macrophage polarization,[30] and EMT can be initiated by TGF-β1 secreted from M2 macrophages through SMAD2 phosphorylation.[27] Accordingly, it is plausible that TGF-β1 and MCP-1 secreted from transplanted fibroblast sheets enhance phosphorylated SMAD2 activation, thereby potentially contributing EMT. Although the majority of transplanted fibroblasts had disappeared by POD 5 (Fig. 1), consistent with earlier reports,[13,15,18] wound healing was promoted in the fibroblast sheet group compared with the controls (Figs. 2 and 3). These observations suggest that multiple factors derived from fibroblast sheets act collectively as triggers for tissue regeneration. Despite the limited survival period of transplanted fibroblast sheets (Fig. 1G), previous studies have reported that dry fibroblast sheets retain therapeutic efficacy in models of cutaneous ulcers and esophageal reconstruction.[31,32] Therefore, the short-term survival of transplanted cells may have a relatively minor influence on the overall regenerative outcome.

Herein, fibroblast cell sheets were transplanted in an allogeneic setting without immunosuppressive treatment. Nevertheless, anastomotic healing showed significant improvement.

Although GFP-positive cells were clearly observed at PODs 0 and 1, they were largely undetectable by POD 5, indicating limited long-term engraftment of transplanted cells (Fig. 1E–H). Therefore, the therapeutic effects of fibroblast sheets are primarily mediated by transient paracrine mechanisms rather than sustained cell survival. This finding aligns with previous reports demonstrating the therapeutic effects of fibroblast sheets in allogeneic environments likely owing to their low immunogenicity and short-term persistence.[13,18]

This study has several limitations. Notably, it includes confirmatory and exploratory elements, which should be considered when interpreting the findings. First, the findings of this study, which used an animal model, may not be completely extrapolated to human tissues or clinical outcomes. Further validation in large animal models is necessary to assess translational applica-

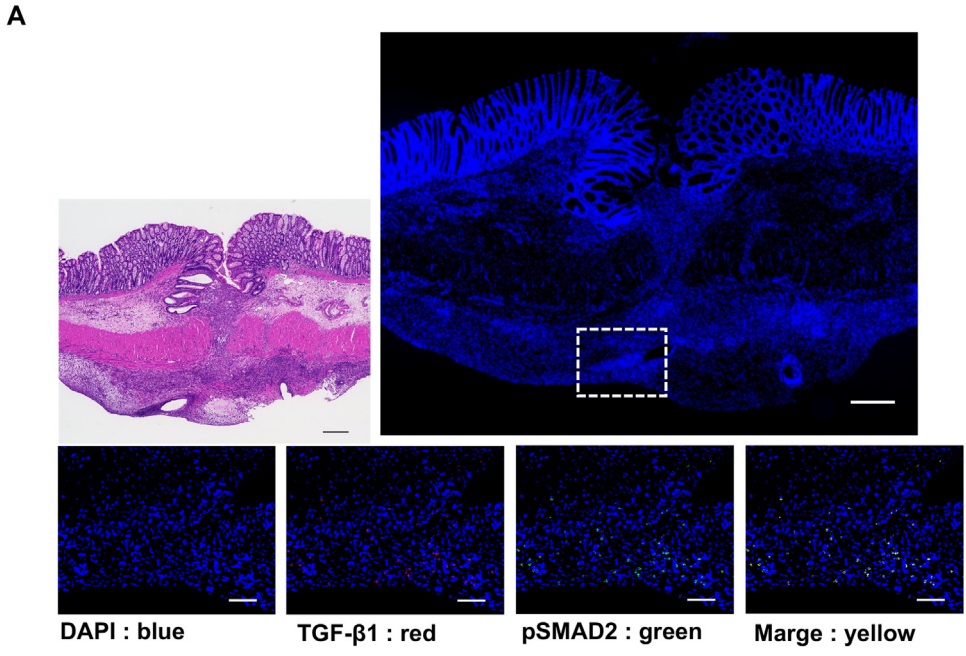

Fig. 6. IF analysis of TGF-β1 and phosphorylated SMAD2 expression at the anastomotic site following cell sheet transplantation. (A) Representative double IF images showing TGF-β1 and phosphorylated SMAD2 expression at the anastomotic site on POD 5. The lower 4 images show an enlarged view of the region within the white dotted line area in the subserosal layer depicted in the upper figure and DAPI-stained nuclei (blue), TGF-β1 (red), phosphorylated SMAD2 (green), and merged double-positive signals (yellow). Scale bars: upper panels, 300 μm; lower panels, 50 μm. (B) High-magnification images of the subserosal layer at the anastomotic site in the control and fibroblast sheet groups, showing DAPI-stained nuclei (blue) and double-positive signals for TGF-β1 and phosphorylated SMAD2 (yellow). (C) The copositive rate was calculated as the proportion of TGF-β1 and phosphorylated SMAD2 double-positive signals relative to the total number of DAPI-positive nuclei. Double-positive signals were quantified in high-power fields on both the oral and anal sides adjacent to the anastomotic center. DAPI-positive nuclei and double-positive signals were automatically quantified using the BZ-X Analyzer software ($n = 4$ per group).

bility. Second, formal randomization and allocation concealment were not implemented, thereby introducing potential selection bias. Future studies with a stricter experimental design are warranted to minimize bias. Third, EMT-like changes suggested by vimentin expression and TGF-β1/pSMAD2 signaling are not specific, and definitive evidence of mesothelial-to-mesenchymal transition was not obtained in this study (Supplementary Fig. 2). Nonetheless, antibody specificity was validated for immunofluorescence staining (Supplementary Fig. 3). Lineage-tracing techniques and additional mesothelial-specific markers are required in future research to clarify the cellular dynamics underlying anastomotic healing. Fourth, a single operator performed all the surgical procedures, thereby potentially introducing operator-related bias, although efforts were made to standardize the technique. Conducting multicenter or multioperator validation studies may improve reproducibility. Fifth, despite standardized surgical procedures, intraluminal contents could not be completely controlled; thus, variability might have been introduced in local mechanical and bacterial stress. More controlled experimental conditions should be considered in future studies. Sixth, no statistically significant difference was observed in bursting pressure, likely attributing to limited statistical power (type II error), as reflected by variability within the control group. Thus, studies with a larger sample size are warranted to confirm these findings and to more precisely estimate effect sizes. Seventh, the observation period was limited to POD 9; consequently, several long-term outcomes, including scar remodeling, adhesion formation, and anastomotic integrity durability, could not be evaluated. Therefore, extended longitudinal studies are necessary. Finally, given the use of allogeneic transplantation, potential immunological interactions between the donor and the recipient cannot be completely ruled out. Further research is needed to clarify the effect of immune responses on therapeutic efficacy.

Moreover, practical challenges for clinical translation, including the standardization of cell sheet fabrication, cryopreservation, storage, and transportation, remain to be addressed.

Conclusion

Frozen–thawed allogeneic multilayered fibroblast cell sheet transplantation reduced anastomotic leakage in a rat colonic anastomosis model and was associated with muscularis gap preservation, suggesting improved structural integrity of the anastomosis. This effect may be attributed to the increased collagen deposition in the subserosal layer.

These findings indicate that this approach is a promising regenerative strategy to enhance anastomotic healing. Although molecular analyses suggested the involvement of TGF-β1/pSMAD2 signaling and EMT-like changes, these mechanisms remain speculative, thereby requiring further investigation.

Further research, including detailed molecular analyses and long-term functional evaluations, is warranted to establish the therapeutic efficacy and clinical applicability of this approach.

Funding

This study was supported by a JSPS Grant-in-Aid for Scientific Research (C) (24K11932 to Y.T.) and a JSPS Grant-in-Aid for Early-Career Scientists (25K19698 to Y.T.). Additional support was provided by the Yamaguchi Prefectural Subsidy Program for the Promotion of Practical Application and Industrialization of Regenerative Medicine (Yamaguchi Prefecture Government to Central Glass Co., Ltd. and Yamaguchi University), the Ube City Subsidy Program for the Promotion of Advanced Research and Development, and the Practical Application of Regenerative Medicine (Ube City Government to Central Glass Co., Ltd. and Yamaguchi University).

Data availability

The datasets supporting this study are publicly available at Zenodo (DOI: https://doi.org/10.5281/zenodo.19866301).

Declaration of competing interest

Koji Ueno, Taro Takami, and Kimikazu Hamano received research funding and consulting fees from Central Glass Co., Ltd. for collaborative research projects. Akihiro Fujita was employed as a research staff member in the Joint Research Course at Yamaguchi University, which was established by Central Glass Co., Ltd. The CY-1 was developed jointly by Central Glass Co., Ltd. and our group at Yamaguchi University. Although the CY-1 substrate was supplied by Central Glass Co., Ltd., the company did not provide any instructions regarding the content of our research. Thus, they played no role in study design, data collection, analysis, interpretation, or manuscript preparation.

Acknowledgments

We gratefully acknowledge Yukari Hironaka for providing exceptional technical support throughout this study. This research was supported by Grants-in-Aid from the Ministry of Education, Culture, Sports, Science, and Technology of Japan, as well as by the Science Research Center, Institute of Life Science and Medicine, and the Institute for Biomedical Research and Education, Yamaguchi University.

Supplementary materials

Supplementary material associated with this article can be found, in the online version, at doi:10.1016/j.cpsurg.2026.102132.

References

1. Boström P, Haapamäki MM, Rutegård J, Matthiessen P, Rutegård M. Population-based cohort study of the impact on postoperative mortality of anastomotic leakage after anterior resection for rectal cancer. *BJS Open*. 2019;3:106–111. doi:10.1002/bjs5.50106.
2. Frasson M, Flor-Lorente B, Ramos Rodríguez JL, et al. Risk factors for anastomotic leak after colon resection for cancer: multivariate analysis and nomogram from a multicentric, prospective, national study with 3193 patients. *Ann Surg*. 2015;262:321–330. doi:10.1097/SLA.0000000000000973.
3. He J, He M, Tang JH, Wang XH. Anastomotic leak risk factors following colon cancer resection: a systematic review and meta-analysis. *Langenbecks Arch Surg*. 2023;408:252. doi:10.1007/s00423-023-02989-z.
4. Rinne JKA, Huhta H, Pinta T, et al. Indocyanine green fluorescence imaging in prevention of colorectal anastomotic leakage: a randomized clinical trial. *JAMA Surg*. 2025;160:486–493. doi:10.1001/jamasurg.2025.0006.
5. Hansen RB, Balachandran R, Valsamidis TN, Iversen LH. The role of preoperative mechanical bowel preparation and oral antibiotics in prevention of anastomotic leakage following restorative resection for primary rectal cancer: a systematic review and meta-analysis. *Int J Colorectal Dis*. 2023;38:129. doi:10.1007/s00384-023-04416-7.
6. Ha GW, Kim HJ, Lee MR. Transanal tube placement for prevention of anastomotic leakage following low anterior resection for rectal cancer: a systematic review and meta-analysis. *Ann Surg Treat Res*. 2015;89:313–318. doi:10.4174/astr.2015.89.6.313.
7. Tan WS, Tang CL, Shi L, Eu KW. Meta-analysis of defunctioning stomas in low anterior resection for rectal cancer. *Br J Surg*. 2009;96:462–472. doi:10.1002/bjs.6594.
8. Ueno K, Takeuchi Y, Samura M, et al. Treatment of refractory cutaneous ulcers with mixed sheets consisting of peripheral blood mononuclear cells and fibroblasts. *Sci Rep*. 2016;6:28538. doi:10.1038/srep28538.
9. Takeuchi Y, Ueno K, Mizoguchi T, et al. Ulcer healing effect of autologous mixed sheets consisting of fibroblasts and peripheral blood mononuclear cells in rabbit ischemic hind limb. *Am J Transl Res*. 2017;9:2340–2351.
10. Mizoguchi T, Ueno K, Takeuchi Y, et al. Treatment of cutaneous ulcers with multilayered mixed sheets of autologous fibroblasts and peripheral blood mononuclear cells. *Cell Physiol Biochem*. 2018;47:201–211. doi:10.1159/000489767.

11. Mizoguchi T, Suehiro K, Ueno K, et al. A pilot study using cell-mixed sheets of autologous fibroblast cells and peripheral blood mononuclear cells to treat refractory cutaneous ulcers. *Am J Transl Res*. 2021;13:9495–9504.
12. Nagase T, Ueno K, Mizoguchi T, et al. Allogeneic fibroblast sheets accelerate cutaneous wound healing equivalent to autologous fibroblast sheets in mice. *Am J Transl Res*. 2020;12:2652–2663.
13. Yamamoto N, Ueno K, Yanagihara M, et al. Allogenic multilayered fibroblast sheets promote anastomotic site healing in a rat model of esophageal reconstruction. *Am J Transl Res*. 2023;15:3217–3228.
14. Iwamoto K, Saito T, Takemoto Y, et al. Autologous transplantation of multilayered fibroblast sheets prevents postoperative pancreatic fistula by regulating fibrosis and angiogenesis. *Am J Transl Res*. 2021;13:1257–1268.
15. Yoshimine S, Tanaka T, Murakami J, et al. Postoperative changes in a bronchial stump following covering with free fat tissue in a rat model. *Eur J Cardiothorac Surg*. 2023;63:ezad154. doi:10.1093/ejcts/ezad154.
16. Ueno K, Ike S, Yamamoto N, et al. Freezing of cell sheets using a 3D freezer produces high cell viability after thawing. *Biochem Biophys Rep*. 2021;28:101169. doi:10.1016/j.bbrep.2021.101169.
17. Suto Y, Ueno K, Kurazumi H, et al. Wound-healing effects of frozen-thawed allogeneic fibroblast sheet transplantation and xenogeneic fibroblast cell sheet transplantation cultured on a new substrate. *Tissue Cell*. 2025;95:102888. doi:10.1016/j.tice.2025.102888.
18. Sakamoto R, Ueno K, Takemoto Y, et al. Development of frozen-thawed allogeneic fibroblast sheets for esophageal anastomotic leakage. *Surgery*. 2025;186:109538. doi:10.1016/j.surg.2025.109538.
19. van der Ham AC, Kort WJ, Weijma IM, Jeekel H. Transient protection of incomplete colonic anastomoses with fibrin sealant: an experimental study in the rat. *J Surg Res*. 1993;55:256–260. doi:10.1006/jsre.1993.1137.
20. van Helsdingen CPM, Wildeboer ACL, Zafeiropoulou K, et al. Histology and transcriptome insights into the early processes of intestinal anastomotic healing: a rat model. *BJS Open*. 2023;7:zrad099. doi:10.1093/bjsopen/zrad099.
21. Bosmans J, Moossdorff M, Al-Taher M, van Beek L, Derikx JPM, Bouvy ND. International consensus statement regarding the use of animal models for research on anastomoses in the lower gastrointestinal tract. *Int J Colorectal Dis*. 2016;31:1021–1030. doi:10.1007/s00384-016-2550-5.
22. Ostrowska-Podhorodecka Z, McCulloch CA. Vimentin regulates the assembly and function of matrix adhesions. *Wound Repair Regen*. 2021;29:602–612. doi:10.1111/wrr.12920.
23. Ostrowska-Podhorodecka Z, Ding I, Norouzi M, McCulloch CA. Impact of vimentin on regulation of cell signaling and matrix remodeling. *Front Cell Dev Biol*. 2022;10:869069. doi:10.3389/fcell.2022.869069.
24. Cheng F, Shen Y, Mohanasundaram P, et al. Vimentin coordinates fibroblast proliferation and keratinocyte differentiation in wound healing via TGF-beta-Slug signaling. *Proc Natl Acad Sci U S A*. 2016;113:E4320–E4327. doi:10.1073/pnas.1519197113.
25. Kasai H, Allen JT, Mason RM, Kamimura T, Zhang Z. TGF-beta1 induces human alveolar epithelial to mesenchymal cell transition (EMT). *Respir Res*. 2005;6:56. doi:10.1186/1465-9921-6-56.
26. Valcourt U, Kowanetz M, Niimi H, Heldin CH, Moustakas A. TGF-beta and the SMAD signaling pathway support transcriptomic reprogramming during epithelial-mesenchymal cell transition. *Mol Biol Cell*. 2005;16:1987–2002. doi:10.1091/mbc.e04-08-0658.
27. Zhu L, Fu X, Chen X, Han X, Dong P. M2 macrophages induce EMT through the TGF-beta/Smad2 signaling pathway. *Cell Biol Int*. 2017;41:960–968. doi:10.1002/cbin.10788.
28. Mutsaers SE. Mesothelial cells: their structure, function and role in serosal repair. *Respirology*. 2002;7:171–191. doi:10.1046/j.1440-1843.2002.00404.x.
29. Weber MC, Clees Z, Buck A, et al. Role of the serosa in intestinal anastomotic healing: insights from in-depth histological analysis of human and murine anastomoses. *BJS Open*. 2024;8:zrae108. doi:10.1093/bjsopen/zrae108.
30. Yang Z, Ma L, Du C, et al. Dental pulp stem cells accelerate wound healing through CCL2-induced M2 macrophage polarization. *iScience*. 2023;26:108043. doi:10.1016/j.isci.2023.108043.
31. Matsuno Y, Yanagihara M, Ueno K, et al. Dry preserved multilayered fibroblast cell sheets are a new manageable tool for regenerative medicine to promote wound healing. *Sci Rep*. 2022;12:12519. doi:10.1038/s41598-022-16345-6.
32. Kurazumi H, Sakamoto R, Ueno K, et al. Anastomotic leakage prevention using dry-preserved fibroblast cell sheets in esophageal reconstruction. *Regen Ther*. 2025;30:795–801. doi:10.1016/j.reth.2025.09.011.